AGU PUBLICATIONS

JGR

Journal of Geophysical Research: Oceans

RESEARCH ARTICLE

10.1002/2017JC013209

Key Points:
- The vertical distribution of solar radiation in the visible domain estimated from models using remote sensing data as input is evaluated
- The best performance was provided by a scheme centered on the Inherent Optical Properties (IOPs)
- The mean uncertainty of the estimated transmittance for a range of 0.1–100% is ~23% from the IOPs system and insensitive to water types

Correspondence to:
M. L. Zoffoli,
laura.zoffoli@umb.edu;
Z. Lee,
zhongping.lee@umb.edu

Citation:
Zoffoli, M. L., Lee, Z., Ondrusek, M., Lin, J., Kovach, C., Wei, J., & Lewis, M. (2017). Estimation of transmittance of solar radiation in the visible domain based on remote sensing: Evaluation of models using in situ data. *Journal of Geophysical Research: Oceans*, *122*, 9176–9188. https://doi.org/10.1002/2017JC013209

Received 29 JUN 2017
Accepted 2 NOV 2017
Accepted article online 10 NOV 2017
Published online 27 NOV 2017

Estimation of Transmittance of Solar Radiation in the Visible Domain Based on Remote Sensing: Evaluation of Models Using In Situ Data

M. Laura Zoffoli[1], Zhongping Lee[1], Michael Ondrusek[2], Junfang Lin[1], Charles Kovach[2,3], Jianwei Wei[1], and Marlon Lewis[4]

[1]School of the Environment, University of Massachusetts, Boston, MA, USA, [2]NOAA/NESDIS/STAR/SOCD, College Park, MD, USA, [3]Global Science & Technology, Greenbelt, MD, USA, [4]Department of Oceanography, Dalhousie University, Halifax, NS, Canada

Abstract The transmittance of solar radiation in the oceanic water column plays an important role in heat transfer and photosynthesis, with implications for the global carbon cycle, global circulation, and climate. Globally, the transmittance of solar radiation in the visible domain (~400–700 nm) (TR_{VIS}) through the water column, which determines the vertical distribution of visible light, has to be based on remote sensing products. There are models centered on chlorophyll-a (Chl) concentration or Inherent Optical Properties (IOPs) as both can be derived from ocean color measurements. We present evaluations of both schemes with field data from clear oceanic and from coastal waters. Here five models were evaluated: (1) Morel and Antoine (1994) (MA94), (2) Ohlmann and Siegel (2000) (OS00), (3) Murtugudde et al. (2002) (MU02), (4) Manizza et al. (2005) (MA05), and (5) Lee et al. (2005) (IOPs05), where the first four are Chl-based and the last one is IOPs-based, with all inputs derived from remote sensing reflectance. It is found that the best performing model is the IOPs05, with Unbiased Absolute Percent Difference (UAPD) ~23%, while Chl-based models show higher uncertainties (UAPD for MA94: ~54%, OS00: ~133%, MU02: ~56%, and MA05: ~39%). The IOPs-based model was insensitive to the type of water, allowing it to be applied in most marine environments; whereas some of the Chl-based models (MU02 and MA05) show much higher sensitivities in coastal turbid waters (higher Chl waters). These results highlight the applicablity of using IOPs products for such applications.

1. Introduction

The amount of the solar radiation in the visible domain (E_{VIS}, 400–700 nm) that reaches deeper depths in the ocean is a key determinant of marine primary production, ocean heating, and vertical mixing (Ohlmann & Siegel, 2000; Schneider et al., 1996). Mathematically, the vertical distribution of E_{VIS} can be described as:

$$E_{VIS}(z) = E_{VIS}(0) \cdot TR_{VIS}(z) \quad (1)$$

with $E_{VIS}(0)$ representing the value just below the sea surface and TR_{VIS} the transmittance of E_{VIS} from surface to depth (z). Symbols used in this work are presented in Table 1.

$E_{VIS}(0)$ is determined by sun position, atmospheric properties, and surface roughness (Frouin et al., 1989) which is beyond the scope of this effort. $TR_{VIS}(z)$, on the other hand, is controlled by properties of water molecules and dissolved and suspended substances in the water. Decades have been spent to easily and accurately describe $TR_{VIS}(z)$. Generally, it can be expressed as:

$$TR_{VIS}(z) = x \cdot e^{-y \cdot z} \quad (2)$$

with x a parameter related to E_{VIS} as a fraction of the total downwelling solar radiation and y a parameter related to water properties.

About a half century ago, the attenuation of E_{VIS} with increasing depth was crudely estimated based on Jerlov water types (Jerlov, 1968), with an *e*-folding depth assigned for each water type. In the 1980s, after the launch of the Coastal Zone Color Scanner (CZCS), efforts shifted to developing models using ocean color

Table 1
Symbols, Description, and Units

Symbol	Definition	Units
a	Absorption coefficient	m^{-1}
A_i	OS00 coefficients for solar transmission parameterizations	Dimensionless
b_b	Backscattering coefficient	m^{-1}
C_{1-4}	OS00 linear regression coefficients for estimation of A_i and K_i	
Chl	Chlorophyll-a concentration	mg m^{-3}
d_{0-4}	MA94 coefficients in the polynomic form to estimate V_{1-2} and z_{1-2} parameters	
e_{Band}	MA05 parameters, either for blue/green or red band	Dimensionless
E_d	Downwelling irradiance measured in water	$\mu W\ cm^{-2}$
$\hat{E}_d$	Downwelling irradiance measured in water corrected for sky variations	$\mu W\ cm^{-2}$
E_S	Downwelling irradiance measured above surface	$\mu W\ cm^{-2}$
K_1, K_2	IOPs05 contributors for the attenuation coefficient at greater depths and subsurface, respectively	m^{-1}
K_{Band}	MA05 attenuation coefficient either for the blue/green or red bands	m^{-1}
K_i	OS00 exponents for solar transmission parameterizations	m^{-1}
K_{VIS}	Attenuation coefficient for VIS radiation	m^{-1}
K_W	Attenuation coefficient for pure water	m^{-1}
Rrs	Remote sensing reflectance	sr^{-1}
V_{1-2}	MA94 partitioning factors	Dimensionless
TR_{IR}	Transmittance in the infrared domain	Dimensionless
TR_{tot}	Transmittance in the whole solar spectrum	Dimensionless
TR_{VIS}	Transmittance in the visible domain	Dimensionless
z	Depth	m
$z_{1\%}$	Depth where E_{VIS} is 1% of its value at surface	m
z_{1-2}	MA94 attenuation lengths	m
λ	Wavelength	nm
θ_S	Solar zenith angle above surface	°
θ_w	Solar zenith angle below surface	°
ζ_{0-2},α_{0-2},χ_{0-2}	IOPs05 parameters for K_{VIS}	Dimensionless
χ_λ	MA05 parameters, either for blue/green or red bands	m^{-2} mg Chl m^{-3}

products to generate seamless distributions of E_{VIS} in the upper water column. In general, the models designed for this estimation can be classified as chlorophyll-a (Chl) concentration based or Inherent Optical Properties (IOPs) based, as both can be adequately derived from the measurements of ocean color. These TR_{VIS} models were evaluated previously using inputs derived from numerical simulations and under these circumstances showed good performance (Lee et al., 2005; Ohlmann & Siegel, 2000). However, for the global oceans, the evaluations of such models using inputs derived solely from ocean color remote sensing are scarce, even though such evaluations are key for the application of satellite ocean color remote sensing.

Note that some of these models are now included in dynamic ocean circulation models to hindcast or forecast stratification of surface waters and heat exchanges between the ocean and atmosphere and between surface and deeper ocean horizons (e.g., Liang & Wu, 2013). It is thus important and necessary to characterize the robustness of such models in estimating $TR_{VIS}(z)$ when the inputs are derived from ocean color. Few widely applied models are tested in this work, based either in Chl or IOPs. The Chl-based models are: Morel and Antoine (1994) (MA94), Ohlmann and Siegel (2000) (OS00), Murtugudde et al. (2002) (MU02), and Manizza et al. (2005) (MA05). The only IOP-based model evaluated is Lee et al. (2005) (IOPs05). The objective of this work is to evaluate the performance of these models using in situ measurements collected in both oceanic and coastal waters. Specifically, we ask two questions. First, when only ocean color measurements are available (represented by remote sensing reflectance, Rrs), can the models provide a robust estimate of TR_{VIS}? Second, which model would in general provide a more reliable estimate for both oceanic and coastal waters?

2. Brief Description of the Models

All the models evaluated here consider exponential decay of solar radiation, but MA94, OS00, and MA05 consist of a form of multiple exponential terms. Key features of these models are highlighted below.

2.1. Morel and Antoine (1994): MA94

Morel and Antoine (1994) developed a TR_{VIS} model as a sum of two exponential functions:

$$TR_{VIS}(Chl, z) = V_1 \cdot e^{-z/z_1} + V_2 \cdot e^{-z/z_2} \quad (3)$$

where $V_{1,2}$ and $z_{1,2}$ are the empirical model parameters of the two terms and they are further described as polynomial functions of Chl

$$V_{1-2}, z_{1-2} = d_0 + d_1 \cdot X + d_2 \cdot X^2 + d_3 \cdot X^3 + d_4 \cdot X^4 \quad (4)$$

$$X = \log(Chl) \quad (5)$$

Here d_{0-4} are the model coefficients determined empirically from simulations for uniform pigment profiles (Morel & Antoine, 1994). MA94 splits the E_{VIS} into two terms without an explict separation of the two spectral regions, but where the first and second terms are for longer and shorter wavelengths, respectively. And, $V_1 + V_2 = 1.0$.

2.2. Murtugudde et al. (2002): MU02

MU02 uses a single exponential term for TR_{VIS}

$$TR_{VIS}(Chl, z) = e^{-z \cdot K_{VIS}} \quad (6)$$

where K_{VIS} (conventionally terms as K_{PAR}) corresponds to the attenuation coefficient of radiation in the visible domain and is expressed as:

$$K_{VIS} = 0.027 + 0.0518 \cdot Chl^{0.428} \quad (7)$$

However, although it was mentioned that this K_{VIS} was based on Morel (1988), K_{VIS} is actually described in Morel (1988) as equation (8):

$$K_{VIS} = 0.121 \cdot Chl^{0.428} \quad (8)$$

Therefore, we evaluated both schemes (equations (7) and (8)) of K_{VIS}, and termed results for K_{VIS} of equation (8) as MU02b.

2.3. Manizza et al. (2005): MA05

Similar to MA94, MA05 also partitions the E_{VIS} transmission into two exponential terms, but then, it divides the full spectrum into two explicit spectral ranges: blue/green (400–599 nm) and red (600–700 nm), with TR_{VIS} as:

$$TR_{VIS}(Chl, z) = 0.5 \cdot e^{-K_{BLUE} \cdot z} + 0.5 \cdot e^{-K_{RED} \cdot z} \quad (9)$$

$$K_{Band} = K_{W,Band} + \chi_{Band} \cdot Chl^{e_{Band}} \quad (10)$$

where K_{BLUE} and K_{RED} are the attenuation coefficients in the blue/green and red bands, respectively, and are also functions of Chl. $K_{W,Band}$, χ_{Band}, and e_{Band} are the model coefficients.

2.4. Ohlmann and Siegel (2000): OS00

The transmission model of Ohlmann and Siegel (2000) is more complicated than the previous Chl-based models. Specifically, OS00 uses not only Chl as input but also the above-surface solar zenith angle (θ_S) (equations (11) and (12)). In addition, OS00 models the transmission for the entire solar radiation (TR_{tot}, ~250–2,500 nm) as the sum of four exponential functions

$$TR_{tot}(Chl, z, \theta_S) = \sum_{i=1}^{4} A_i \cdot e^{-K_i \cdot z} \quad (11)$$

with A_i and K_i modeled as functions of Chl

$$A_i, K_i = C_1 \cdot Chl + C_3 \cdot \left(\cos(\theta_S)\right)^{-1} + C_4 \quad (12)$$

Here C_{1-4} are model coefficients that were determined empirically from numerical simulations (Ohlmann & Siegel, 2000). In addition, OS00 considered the impacts of clouds, but here we used the model of clear sky only.

Since here the focus is the transmission of E_{VIS}, the above model is converted to TR_{VIS} as:

$$TR_{VIS}(Chl, z, \theta_S) = (TR_{tot} - TR_{IR})/0.47 \quad (13)$$

In equation (13), the value 0.47 represents the fraction of the solar radiation corresponding to the visible domain, i.e., ~47% of the total solar radiation (Frouin et al., 1989). TR_{IR} is the transmittance for solar radiation in the ~700–2,500 nm range and approximated as that in Morel and Antoine (1994)

$$TR_{IR} = e^{-\frac{3.75 \cdot z}{(\cos(\theta_W))}} \quad (14)$$

where θ_w is the solar zenith angle below sea surface.

2.5. Lee et al. (2002): IOPs05

The transmittance of solar radiation is determined by optical properties (absorption and scattering coefficients). Because the conversion coefficients between Chl and IOPs are spatially and temporally dependent, Lee et al. (2005) developed a transmission model centered on IOPs in order to avoid the conversion from Rrs to Chl, and then from Chl to optical properties.

Specifically, IOPs05 models TR_{VIS} as

$$TR_{VIS}(IOP, z, \theta_S) = e^{-K_{VIS}(IOP, z, \theta_S) \cdot z} \quad (15)$$

where K_{VIS} is modeled as a function of depth and IOPs,

$$K_{VIS}(IOP, z, \theta_S) = K_1(IOP, \theta_S) + \frac{K_2(IOP, \theta_S)}{(1+z)^{0.5}} \quad (16)$$

$$K_1(IOP, \theta_S) = \left[\chi_0 + \chi_1 \cdot (a(490))^{0.5} + \chi_2 \cdot b_b(490)\right](1 + \alpha_0 \cdot \sin(\theta_S)) \quad (17)$$

$$K_2(IOP, \theta_S) = [\zeta_0 + \zeta_1 \cdot a(490) + \zeta_2 \cdot b_b(490)](\alpha_1 + \alpha_2 \cdot \sin(\theta_S)) \quad (18)$$

where $a(490)$ and $b_b(490)$ are the absorption and backscattering coefficients at 490 nm, with χ_{0-2}, α_{0-2}, and ζ_{0-2} derived empirically from numerical simulations (Lee et al., 2005).

3. Data Used for TR_{VIS} Evaluation

3.1. In Situ Data Collection

Two in situ data sets were included in this work covering conditions ranging from extremely clear oceanic to turbid coastal waters. One was obtained during NOAA Visible Infrared Imaging Radiometer Suite (VIIRS) validation cruises (VIIRS data set) and the other during the Biogeochemistry and Optics South Pacific Experiment (BIOSOPE data set).

The VIIRS cruises were conducted in three consecutive years: VIIRS-2014 (11–20 November), VIIRS-2015 (2–13 December), and VIIRS-2016 (14–19 October). The stations of these cruises were located mainly in coastal waters, encompasing waters in the North Atlantic Ocean and Bahamas (Figure 1). The measurements were taken during different environmental conditions, such as sea state, sky condition, and θ_S (42–74°) as well as in waters with different Chl concentrations (ranging from ~0.2 to 11.4 mg m^{-3}, estimated from in situ Rrs with the NASA algorithm) and IOPs properties. A HyperPro free-falling optical profiler was used to measure hyperspectral downwelling irradiance (E_d, μW cm^{-2} nm^{-1}) between 350 and 800 nm throughout the water column. A total of 35 stations collected during these VIIRS cruises were applicable for this effort, with profiling depths down to ~17 m. Additionally, above-surface hyperspectral remote sensing reflectance (Rrs(λ), sr^{-1}) was obtained using a floating HyperPro radiometer system, adapted with a Skylight Blocking Apparatus (SBA system, Lee et al., 2013a). The HyperPro and SBA systems were deployed at a minimum distance of 20 m from the operating boat to avoid any contamination from the ship in the measurements. SBA recorded data for 5–10 min at each station in the same spectral range as the profiling HyperPro radiometer (350–800 nm). Measurements with a tilt greater than 5° were excluded. Derivation of Rrs(λ) from the SBA scheme followed the procedure detailed in Lee et al. (2013a) and Wei et al. (2015).

The BIOSOPE cruise was carried out during the austral summer of 2004 (3 November to 10 December). This cruise covered waters from the South Pacific Gyre to coastal waters in the Continental Shelf of Chile. E_d

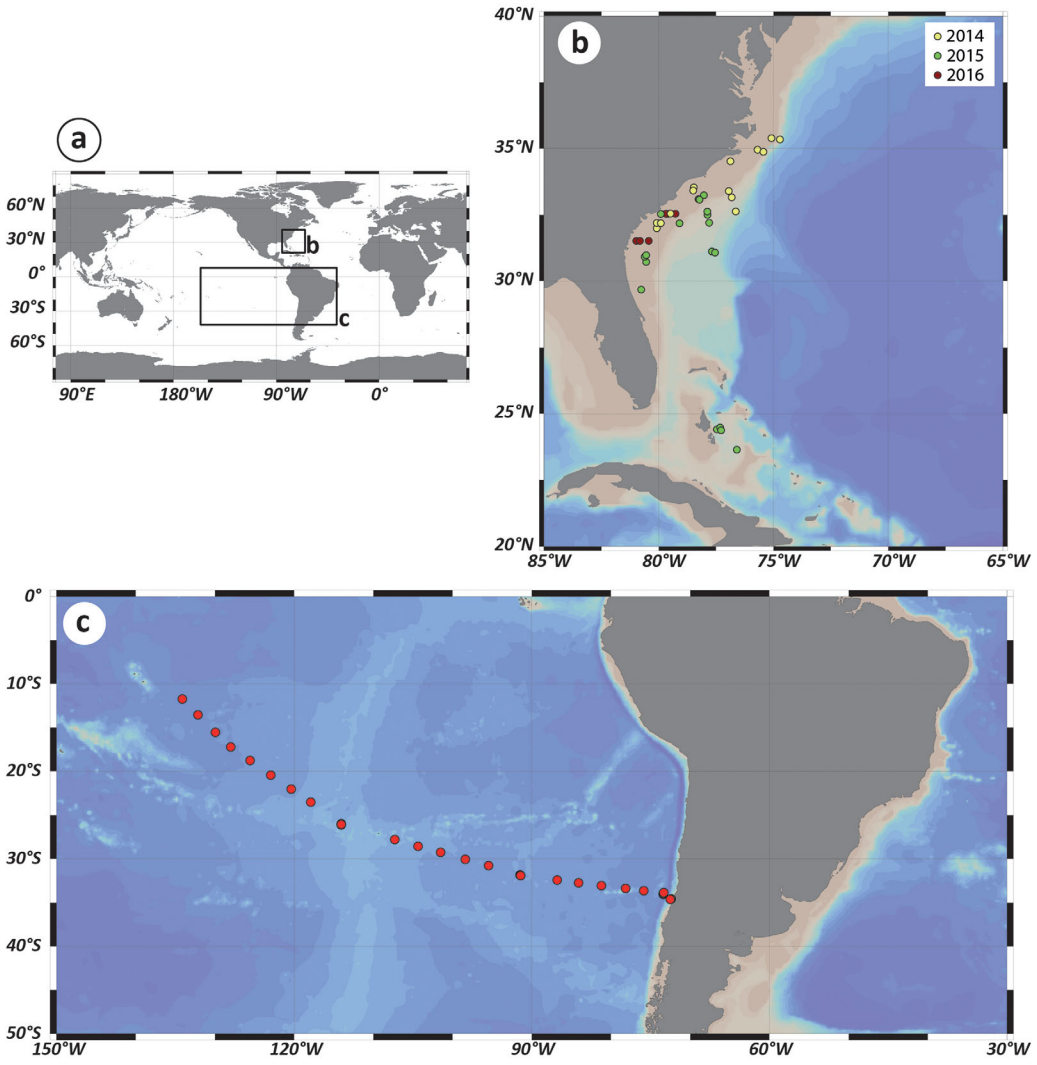

Figure 1. (a) Location of the stations in a global context defined during the (b) VIIRS Cal-Val cruises and (c) BIOSOPE cruise.

profiles were measured using a HyperPro free-falling optical profiler. Because the waters were very clear, the profiles were much deeper (as deep as 193 m). The measurements were taken between 9:00 and 16:00 local time, with θ_S in a range of 7–48°. Rrs(λ) was derived from the HyperPro measurements using the ProSoft software. A total of 22 stations were applicable for this effort.

3.2. Processing of Hyperspectral Profiling Measurements for TR_{VIS}

It is critical to obtain field measurements of TR_{VIS} data that is accurate as possible for the evaluation of the various schemes for TR_{VIS} estimation from remote sensing. The derivation of in situ TR_{VIS} consisted of several sequential steps (see Figure 2). Specifically,

1. E_d profiles were processed following the recommendations in the NASA protocols (NASA, 2003).
2. In order to remove cloud effects, the normalized E_d ($\hat{E}_d(\lambda, z)$) was estimated as follows:

$$\hat{E}_d(\lambda, z) = \frac{E_d(\lambda, z, t_z) \cdot E_S(\lambda, t_i)}{E_S(\lambda, t_z)} \tag{19}$$

where E_S corresponds to the downwelling irradiance measured above-water, t_i corresponds to the time when the profiling HyperPro radiometer is at the surface and t_z is the profiling HyperPro radiometer time at depth z.

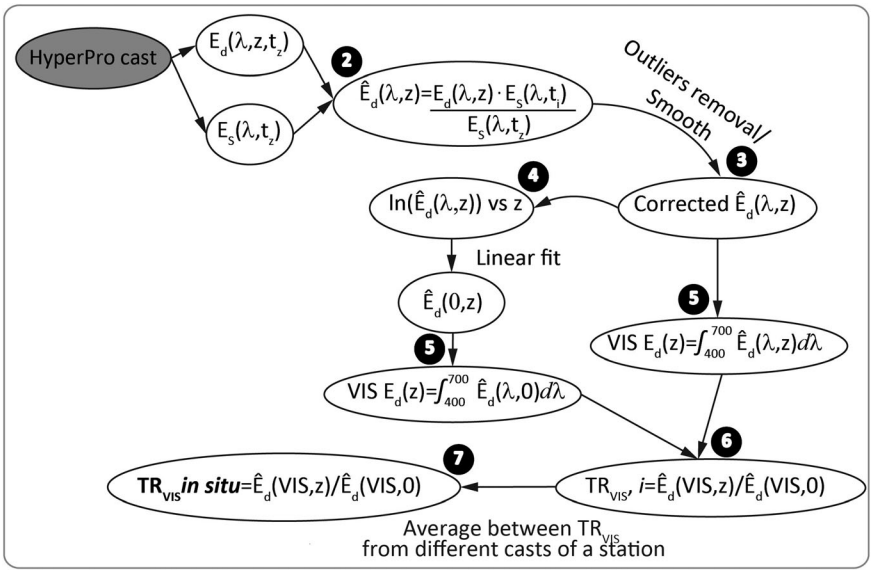

Figure 2. Flowchart showing the data processing applied to obtain modeled and in situ TR_{VIS}.

3. $\hat{E}_d(\lambda,z)$ profiles were very noisy, especially in the first few meters, typically a result of the wave focusing effect (Wei et al., 2014; Zaneveld et al., 2001; Zibordi et al., 2004). The noise was uncorrelated between bands, profiles, and stations. In our data processing, for every cast, $\hat{E}_d(\lambda,z)$ profiles of every band were visually inspected and outliers of $\hat{E}_d$ at depth were removed. Subsequently, a moving average filter was used to smooth the profiles.
4. The smoothed profiles were used to estimate the normalized downwelling irradiance measured below surface ($\hat{E}_d(\lambda,0)$) from the linear fit between $\ln \hat{E}_d(\lambda,z)$ and z (Smith & Baker, 1984, 1986).
5. Both $\hat{E}_d(\lambda,0)$ and $\hat{E}_d(\lambda,z)$ were integrated spectrally over the 400–700 nm range to produce $\hat{E}_d(VIS)$.
6. TRVIS for each cast was subsequently calcualted as $\hat{E}_d(VIS,z)/\hat{E}_d(VIS,0)$.
7. Finally, if there were multiple casts, TRVIS of a station was an average of the transmittance obtained from each cast.

3.3. Input Properties for TR_{VIS} Estimations

In situ Rrs(λ) was used to model TR_{VIS} when using the Chl or the IOPs method. Chl was estimated applying the Chl_{OCI} algorithm of Hu et al. (2012). IOPs values (a(490) and b_b(490)) were calculated by version 6 of the Quasi-Analytical Algorithm (QAA v6) (Lee, 2014; Lee et al., 2002). For this derivation, Raman correction was implemented following the method described in Lee et al. (2013b).

3.4. Uncertainty Analyses

TR_{VIS} was evaluated at 1 m intervals for all of the stations and for values of in situ $TR_{VIS} > 0.001$ (0.1%). TR_{VIS} of deeper depths is associated with higher uncertainties so was excluded in such evaluations. Several statistical measures were employed to evaluate the differences between in situ and calculated TR_{VIS} for every model: Unbiased Percent Difference (UPD) (equation (20)), Unbiased Absolute Percent Difference (UAPD) (equation (21)), Root Mean Square Difference (RMSD) (equation (22)), and coefficient of determination (R^2)

$$UPD\,(\%)=2\cdot(x_{mod}-x_{mea})/(x_{mod}+x_{mea})\cdot 100 \tag{20}$$

$$UAPD\,(\%)=2\cdot|(x_{mod}-x_{mea})|/(x_{mod}+x_{mea})\cdot 100 \tag{21}$$

$$RMSD=\sqrt{\frac{\sum(x_{mod}-x_{mea})^2}{N}} \tag{22}$$

where x_{mod} and x_{mea} represent the TR_{VIS} values derived from models and measured in situ, respectively.

4. Results

Estimated TR_{VIS} values using either IOPs or Chl as inputs, which are standard products in the ocean color remote sensing, were compared with in situ TR_{VIS} values. A summary of these comparisons can be found in Table 2 and Figure 3. Not surprisingly, due to different mathematical functions and model coefficients, there are also large differences in the performances among the Chl-based models, at least for this data set. Considering all the samples, we observe that:

1. For TR_{VIS} in a range of ~100% (near surface) to 0.1% (deeper depths), it is found that MA94 and MA05 performed best among the Chl-based models. Statistically, the two models had UAPD values of 54.1% and 38.9%, and root mean square differences (RMSD) of 0.058 and 0.043, respectively. MA94 tended to underestimate TR_{VIS} (UPD, −42.9%); while MA05 showed an even lower underestimation of TR_{VIS} (UPD, −9%), while the dispersion of the modeled TR_{VIS} values was not depth dependent. These results highlight the importance of using multiple exponential functions for the description of TR_{VIS}, if the attenuation coefficient for each exponential function is kept as a constant vertically. This is fundamentally because the attenuation coefficient of water is spectrally dependent and different spectral bands are associated with different relationships with the optically active constituents in water.
2. OS00 and MU02 showed poorer performance, considering both had high UAPD (132.7% and 55.5%, respectively) and high RMSD values (0.081 and 0.116, respectively). These two models presented different patterns in the predicted TR_{VIS} values. On average, OS00 significantly underestimated TR_{VIS} (UPD, −128.3%) but it overestimated TR_{VIS} for the highest TR_{VIS} values (shallowest depths) and presented the highest dispersion for TR_{VIS} values between ~0.1 and 0.6. MU02, on the contrary, displayed a hyperbolic behavior with maximum deviation from the 1:1 line for intermediate TR_{VIS} values (between ~0.2 and 0.8). Even though the mean UAPD was close to 0, the UAPD value was much higher compared to MA05. This shows that there was a compensation between positive and negative UAPD values when the average was calculated. MU02 tended to overestimate TR_{VIS} for high values and underestimated TR_{VIS} for values lower than 0.2 in clear waters. This is actually expected when TR_{VIS} is expressed as a single exponential function along with a vertically constant K_{VIS} (Lee, 2009). This is because K_{VIS} used for the development of the empirical relationships were generally calculated between the surface and a depth where E_{VIS} is close to 1% of the surface value ($z_{1\%}$), and this K_{VIS} is significantly smaller than K_{VIS} above $z_{1\%}$ for oceanic waters (Lee, 2009). Therefore, an overestimation of TR_{VIS} will result when K_{VIS} of smaller values are used (between surface and a much deeper depth).

Figure 3d shows the comparison of TR_{VIS} from MU02b with in situ TR_{VIS} when $K_{VIS} = 0.121\ Chl^{0.428}$ was employed. MU02b showed a slightly worse performance than MU02, with UAPD of 70.0% and had significant overestimations. Again, this overestimation is due to the fact that K_{VIS} between the surface and $z_{1\%}$ is generally smaller than K_{VIS} from a shallower depth range (Lee, 2009).

1. IOPs05 exhibited the best performance among the models evaluated here, with the lowest UAPD (22.8%), lowest RMSD (0.022), and lowest dispersion (highest R^2) between predicted and measured TR_{VIS} values. In particular, the performances for low Chl or high Chl waters were nearly the same, i.e., it is nearly universally applicable. It is recalled that, on the contrary of the previous tested models, in this model TR_{VIS} is derived directly from optical properties, such as absorption and backscattering. Its good performance derives then from two important factors: (i) K_{VIS} in IOPs05 is a function of depth as highlighted in

Table 2
Coefficients to Evaluate Model Uncertainties: R^2, Mean Unbiased Percent of Difference (UPD, in %), Range and Mean of Unbiased Absolute Percent of Difference (UAPD, in %) and Root Mean Square Difference (RMSD)

	R^2	Mean UPD (%)	Range UAPD (%)	Mean UAPD (%)	RMSD
MA94	0.96	−42.9	0–161.3	54.1	0.058
OS00	0.90	−128.3	0–199.9	132.7	0.081
MU02	0.91	−0.9	0–190.2	55.5	0.116
MU02b	0.94	68.5	0–174.4	70.0	0.137
MA05	0.95	−9.0	0–166.8	38.9	0.043
IOPs05	0.99	1.6	0–152.8	22.8	0.022

Note. These coefficients were evaluated for in situ $TR_{VIS} > 0.001$.

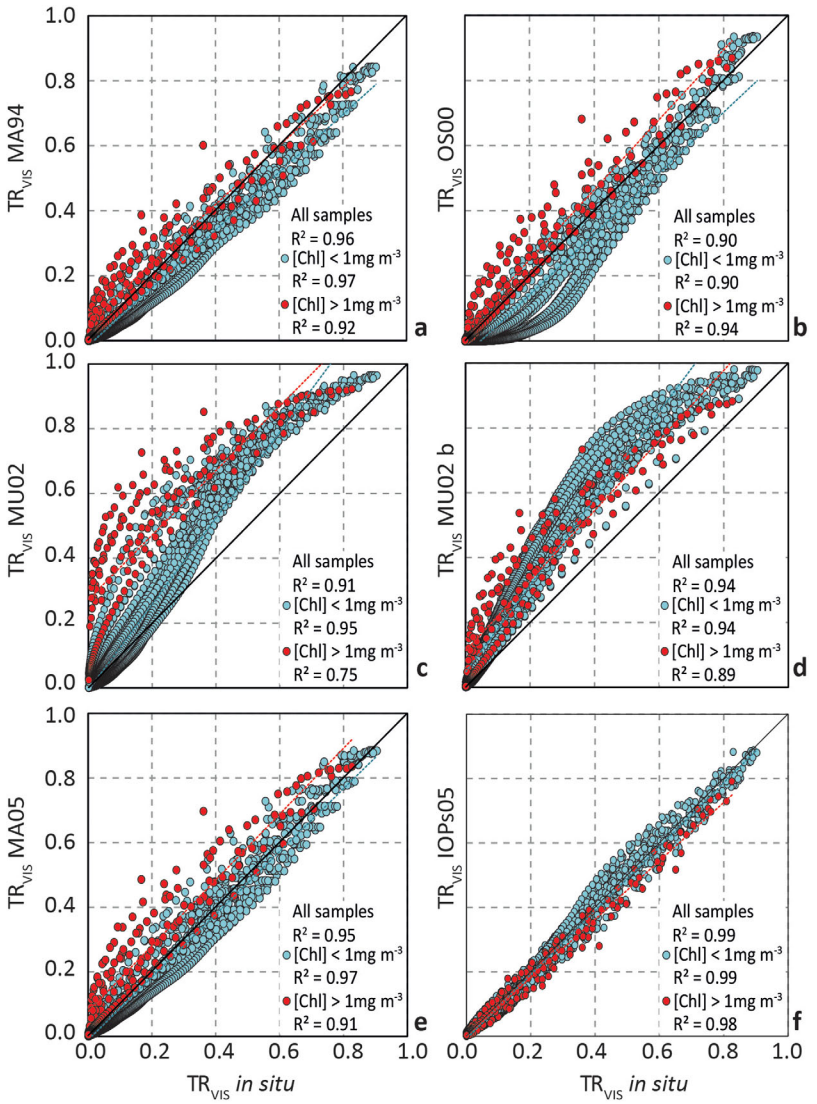

Figure 3. Calculated TR_{VIS} versus measured TR_{VIS} from in situ data. TR_{VIS} derived from different models are displayed: (a) MA94, (b) OS00, (c) MU02, (d) MU02b, (e) MA95, and (f) IOPs05. Each data set was divided into TR_{VIS} estimated in waters with Chl < 1 mg m^{-3} (light blue dots) and Chl > 1 mg m^{-3} (red dots).

Lee et al. (2005) and Lee (2009). (ii) This K_{VIS} is modeled as a function of IOPs, not Chl, thus it avoids the uncertainties associated with the conversion between biological and optical properties such as the specific absorption coefficient of chlorophyll or phytoplankton (Bricaud et al., 1995). Note that when K_{VIS} is modeled as a function of Chl, inevitably, there will be assumptions in the relationships between IOPs and Chl, which vary spatially and temporally, but these assumed relationships do not necessarily match waters of a specific location or time.

2. When the distribution of UAPDs was analyzed, it was found that around 75% of the TR_{VIS} values predicted by IOPs05 were within 30% of in situ TR_{VIS} (Figure 4). MA05 displayed the best performance among the Chl-based models, with around 41% of the stations having uncertainties within 30%. MA94 presented errors up to 30% in around 33% of the cases while for MU02 uncertainties were up to 30% in 27% of the cases. The poorest performances were exhibited by OS00 and MU02b, with differences higher than 100% in 68% and 18% of the cases, respectively.

The Chl-based models generally assume that the variation of light attenuation can be modeled as a function of Chl, where all the active optical properties co-vary with phytoplankton, i.e., the so-called "Case 1" waters.

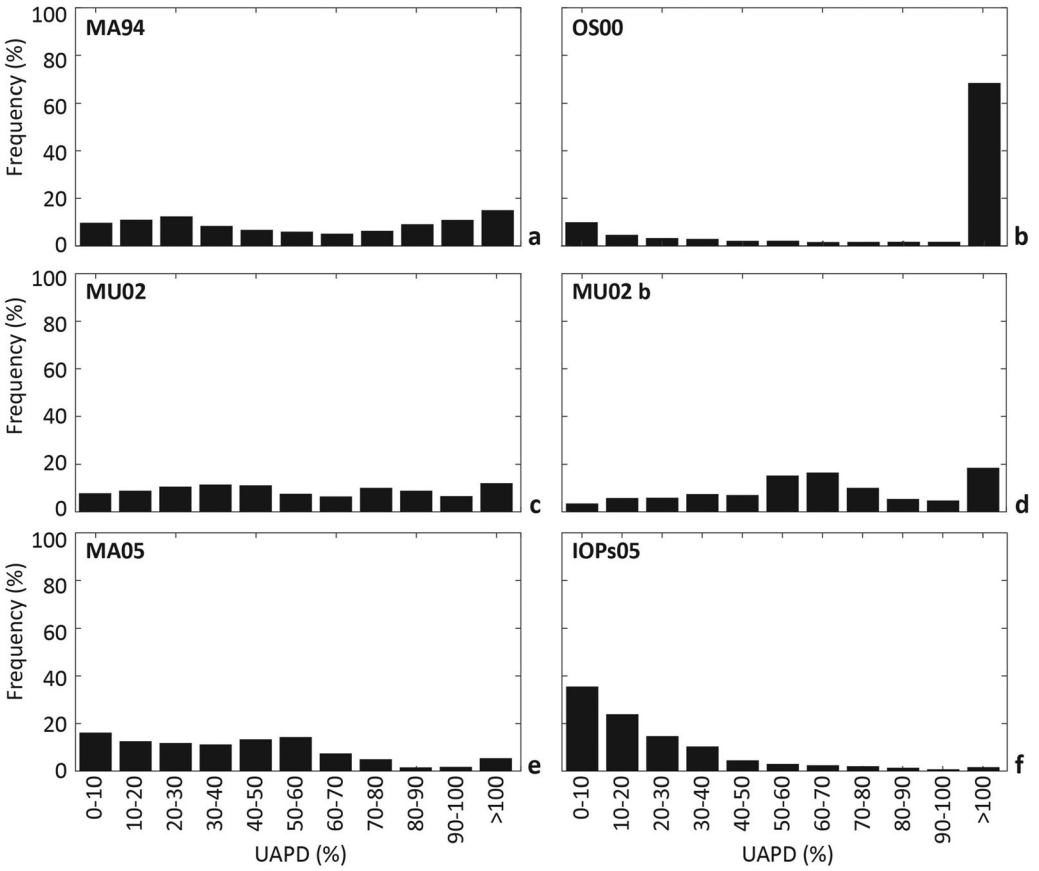

Figure 4. Frequency of the Unbiased Absolute Percent Difference (UAPD, %) for the evaluated TR_{VIS} models: (a) MA94, (b) OS00, (c) MU02, (d) MU02b, (e) MA95, and (f) IOPs05.

Here there was not enough information to evaluate which stations corresponded to the "Case 1" category. Therefore for further analysis, the in situ data set was divided into two groups with one group for Chl $>$ 1 mg m^{-3} (13 stations) and the other group for Chl $<$ 1 mg m^{-3} (44 stations). It was found that (see Figure 3 and Table 3):

1. The Chl-based models showed a systematic overestimation of TR_{VIS} for high Chl waters. For low Chl waters, MA94 slightly underestimated TR_{VIS} while MA05 provided the best results among the Chl-based schemes. MA94 and OS00 actually performed better for higher Chl waters than lower Chl waters. The reasons behind this contrast in performance are not clear. In the case of OS00, it could be due to its formation of multiple exponential functions and a large number of model parameters. The MA05 clearly performed better for low Chl waters than higher Chl waters. One possible reason is that the higher Chl waters (which generally are coastal for this data set) likely encountered contributions from colored dissolved organic matter or suspended sediments that cannot be well described from the empirically derived Chl.
2. The IOPs05 model, however, generally showed no dependence on the range of Chl, although it appears that there was an overestimation (up to ~20%) of TR_{VIS} when TR_{VIS} was in the ~0.4–0.6 range for lower Chl waters. This will require further study to understand the underlying reasons. Generally, for both low and high Chl groups the mean UAPD for IOPs05 were ~23–25%. Again, these comparisons demonstrate the advantages of using IOPs to model and predict the vertical distribution of E_{VIS} in the upper water column.

Table 3
Absolute Unbiased Percent Difference (UAPD, in %), Between In Situ TR_{VIS} and Calculated TR_{VIS} From Different Models

	Mean UAPD All stations	Mean UAPD Chl $<$ 1 mg m^{-3}	Mean UAPD Chl $>$ 1 mg m^{-3}
MA94	54.1	53.4	27.5
OS00	132.7	136.5	31.9
MU02	55.5	53.6	106.7
MU02b	70.0	69.3	69.2
MA05	38.9	38.0	57.1
IOPs05	22.8	22.7	25.0

Note. Included are estimations for the whole data set (all stations) and for stations grouped according to Chl (1 mg m^{-3} $>$ Chl $>$ 1 mg m^{-3}).

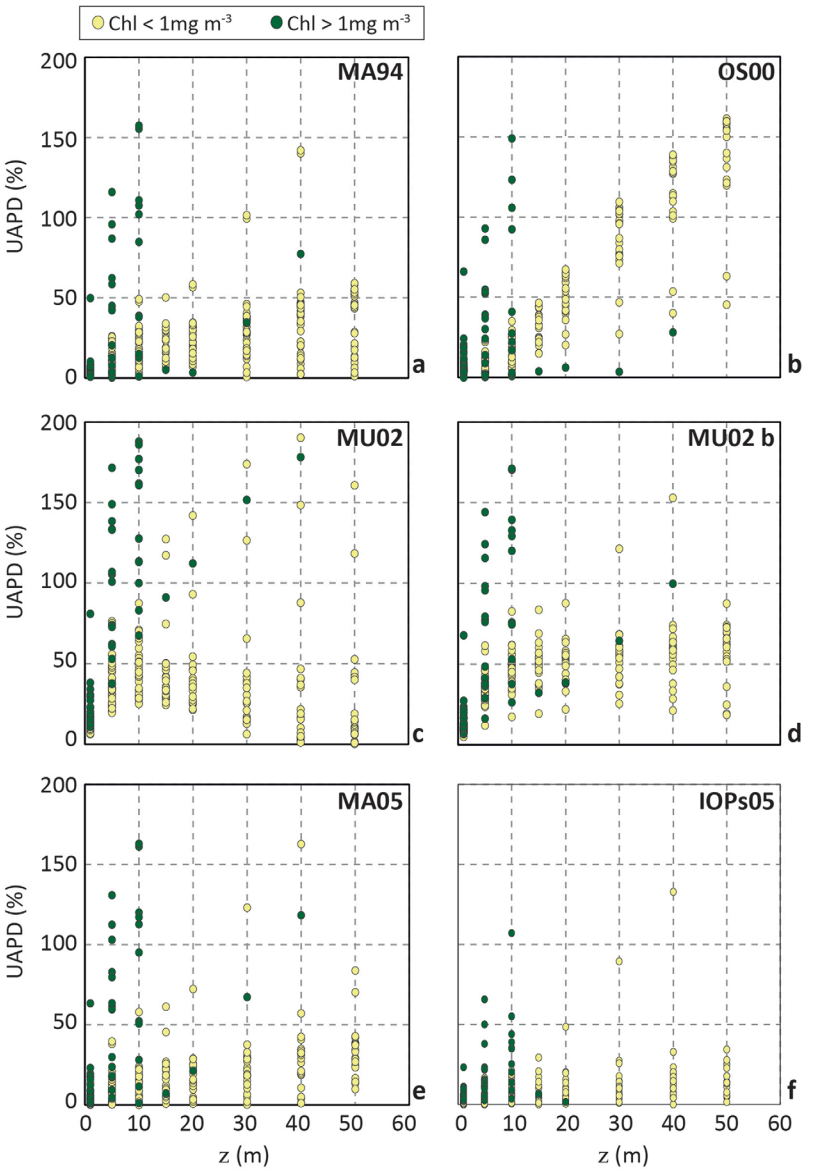

Figure 5. UAPD (%) of the TR_{VIS} derived from different models as a function of depth (z, m): (a) MA94, (b) OS00, (c) MU02, (d) MU02b, (e) MA95, and (f) IOPs05. Each data set was divided into UAPD estimated in waters with Chl < 1 mg m^{-3} (yellow dots) and Chl > 1 mg m^{-3} (green dots).

All of these evaluations and comparisons indicate that (1) the way of modeling TR_{VIS} is important (e.g., vertically constant K_{VIS} versus vertically varying K_{VIS}; one exponential term versus multiple exponential terms) and (2) it is more robust to estimate TR_{VIS} based on IOPs, rather than based on Chl, as Chl is just one of the active components that can affect the optical properties of bulk water.

Because ocean circulation models calculate solar radiation to specific depths in the upper water column (Sweeney et al., 2005), we also evaluated the model performance in some discrete depths (at 1, 5, 10, 15, 20, 30, 40, and 50 m, respectively), with TR_{VIS} values limited to greater than 0.001 (Figure 5). Again, while models based on Chl (even for Chl < 1 mg m^3) could have many estimations of TR_{VIS} with an uncertainty more than 50% (especially OS00 and MU02), uncertainties by IOPs05 were generally less than 50% for all waters and depths. These results imply that the modeled upper water heating and dynamics based on remotely estimated Chl should be revised.

5. Discussion

In this work, for the first time we carried out a systematic evaluation regarding the estimation of TR_{VIS} when inputs for such models are only available from ocean color remote sensing, a route to apply these models to global waters. At least for this data set, the IOPs05 model performs better than other models evaluated. It has the lowest mean UAPD (around 23%) and the lowest RSMD. Around 75% of the cases have differences compared with in situ measurements within 30% and are insensitive to high Chl levels, as often occur in coastal waters. Comparing the performances among the Chl-based models, looking at the mean, range, and frequency of the UAPD, the best performance was exibited by the MA94 and MA05, which split the visible spectrum into two regions with two exponential terms to estimate TR_{VIS}. Models adopted as MU02, with a single exponential function for the whole visible spectrum along with a vertically constant K_{VIS}, did not perform as well when describing the vertical distribution of E_{VIS} in the water column. Note that among the TR_{VIS} models evaluated, the complexity and computational efficiency are not significantly different, and there is no relationship between complexity and performance.

In this work, in situ TR_{VIS} was calculated strictly for the spectral range of 400–700 nm, the same window as MU02b and MA05, and almost the same as MU02 (380–700 nm). The other evaluated models, however, used slightly different spectral ranges although all are considered within the visible domain. For instance, some of them include some portion of the near-UV (in the range 300–400 nm) or near-IR (700–750 nm). To evaluate the impact of such difference in wavelengths on TR_{VIS}, simulations by HydroLight (Mobley & Sundman, 2008) were carried out with Chl as 0.05, 0.5, and 5 mg m^{-3} (following the default Case-1 model in HydroLight) for the upper 50 m. It is found that the differences between TR_{VIS}(400–700) and TR_{VIS}(300–750) were very small ($\sim$6%) for low Chl ($\leq$0.5 mg m^{-3}) in the whole water column, with TR_{VIS}(400–700) generally greater than TR_{VIS}(300–750) due, in general, to higher absorption coefficients in the 350–400 and 700–750 nm spectral windows. It is thus clear that the difference in spectral ranges has limited effect on the comparison of model performances. Separately, the contribution of solar radiation in the 350–400 nm window to $E_{VIS}(0)$ is small ($<\sim$2%) while the contribution in the 700–750 nm window to $E_{VIS}(0)$ is accounted for in other models (e.g., Lee et al., 2005), thus using the 400–700 nm window to represent TR_{VIS} will not affect the heating effect in dynamic models as long as the entire short-wave solar radiation is accounted for properly.

For Chl-based models, despite the moderate performance exhibited by the MA05 (UAPD $\sim$ 40%), it should be taken into account that when Chl is higher, errors higher than 100% could be expected (TR_{VIS} values can be $\sim$1–30%). This model showed sensitivity to Chl as its performance was reduced in waters with Chl $>$ 1 mg m^{-3}, at least for the data evaluated here. Fundamentally, the MA05 model was designed for Case-1 waters, where Chl is the primary driving force of the change of optical properties. Lee and Hu (2006) showed that likely only 60% of the global oceans follows strictly the bio-optical relationships of Case-1 waters, whose spatial variation changes seasonally and their boundaries are difficult to establish. In particular, the definition of Case-1 waters is not based on latitude and/or longitude, rather it is based on optical dependences; thus, it is difficult to know if a water body belongs to Case-1 based on remote sensing reflectance (Lee & Hu, 2006). As a result, if models are sensitive to Chl, it may not be appropriate to use such models in some regions or at some seasons, for example, during phytoplankton blooms. This might also be a reason why Manizza et al. (2005) suggested improving their TR_{VIS} model by including bio-optical parameterizations for each phytoplankton functional type (PFT). However, as demonstrated in Lee et al. (2005) and here, the propagation of light depends on bulk optical properties, and such properties can be well estimated from radiometric measurements (Lee et al., 2005; Werdell et al., 2013) and there is no need to know a priori biological properties of the environment, such as the dominant PFT.

Errors or uncertainties in getting Chl and IOPs from Rrs are beyond the scope of this study. Here the focus is on the Rrs to TR_{VIS} system because inputs for TR_{VIS} could only be obtained on a global scale from Rrs. In particular, at least for the Chl-based models, it is the same Chl derived from Rrs used to estimate TR_{VIS} of the various water bodies; and further it is the same Rrs used as input for the TR_{VIS} estimations of all models. Note that for satellite ocean color remote sensing, Rrs is a first-order product of the targeted water bodies. Although it is not clear if Chl or IOPs derived from Rrs are highly accurate, our results exhibited that the direct use of optical properties, a and b_b, reduces the uncertainties in the estimated TR_{VIS}. Further, although some uncertainties are associated with the estimation of the IOPs (Lee et al., 2010; Werdell et al., 2013), the

results here show that the TR_{VIS} estimated with the IOPs model can be accurate to within ~20% when it is derived simply from Rrs. Shulman et al. (2017) recently showed that coupled errors between the estimation of TR_{VIS} and $E_{VIS}(0)$ can significantly affect the modeled heat exchange in the water column. Thus, an accurate TR_{VIS} model will reduce one of the error sources in ocean dynamic and climate models.

Note that the model comparison performed here considered only in situ information, without any interaction with the atmosphere. However, for satellite ocean color remote sensing, the atmosphere contributes around 90% of the total signal at the top of the atmosphere (IOCCG, 2010). Thus, atmospheric correction is an essential step in obtaining accurate Rrs and then IOPs. Even for the model based on IOPs, it is necessary to evaluate $E_{VIS}(z)$ when all the input parameters are derived from satellite ocean color measurements.

6. Conclusions

Modeling the propagation of visible solar radiation (TR_{VIS}) in the upper water column is important for the study of heating and photosynthesis of the global oceans, whereas the input for such models has to be derived from ocean color remote sensing. Here, for the first time, TR_{VIS} was evaluated with data measured in both oceanic and coastal waters. It was found that the best performing model is based on inherent optical properties (IOPs05), where a mean uncertainty of ~23% is obtained for TR_{VIS} in a range of 0.1–100%, and this model is not sensitive to water types. The models (MA94 and MA05) showed the lowest uncertainties among the Chl-based models and presented differences in performance depending on the Chl concentration, indicating high dependence on the relationships between optical properties and Chl. Because TR_{VIS} is an optical property, the results here further advocate the adoption of bulk IOPs for accurate estimation of TR_{VIS}, which could have significant impact on the modeling of heating and photosynthesis in the upper water column.

Acknowledgments
Financial support was provided by the National Oceanic and Atmospheric Administration (NOAA) JPSS VIIRS Ocean Color Cal/Val Project (NA11OAR4320199), the National Aeronautic and Space Administration (NASA) Ocean Biology and Biogeochemistry and Water and Energy Cycle Programs (NNX14AK08G, NNX14AQ47A, NNX14AM15G). We thank the crew of R/V *Nancy Foster* for their dedicated and professional support for the field measurements. Data are available at http://oceanoptics.umb.edu/files/2016/03/TRVIS_Zoffoli_et_al_2017-w0mw54.xlsx.

References

Bricaud, A., Babin, M., Morel, A., & Claustre, H. (1995). Variability in the chlorophyll-specific absorption coefficients of natural phytoplankton: Analysis and parameterization. *Journal of Geophysical Research*, *100*(C7), 13321–13332. https://doi.org/10.1029/95JC00463

Frouin, R., Lingner, D. W., Gautier, C., Baker, K. S., & Smith, R. C. (1989). A simple analytical formula to compute clear sky total and photosynthetically available solar irradiance at the ocean surface. *Journal of Geophysical Research*, *94*(C7), 9731. https://doi.org/10.1029/JC094iC07p09731

Hu, C., Lee, Z., & Franz, B. (2012). Chlorophyll a algorithms for oligotrophic oceans: A novel approach based on three-band reflectance difference. *Journal of Geophysical Research*, *117*, C01011. https://doi.org/10.1029/2011JC007395

IOCCG (2010). Atmospheric correction for remotely-sensed ocean-colour products. In M. Wang (Ed.), *Reports of the International Ocean-Colour Coordinating* (Group 10). IOCCG: Dartmouth, Canada.

Jerlov, N. G. (1968). *Optical oceanography* (194 pp.). Amsterdam, Netherlands: Elsevier.

Lee, Z. (2009). KPAR: An optical property associated with ambiguous values. *Journal of Lake Sciences*, *21*(2), 159–164.

Lee, Z. (2014). *Update of the Quasi-Analytical Algorithm (QAA_v6)*. International Ocean Colour Coordinating Group, Dartmouth, Canada. Retrieved from http://www.ioccg.org/groups/Software_OCA/QAA_v6_2014209.pdf

Lee, Z., Arnone, R., Hu, C., Werdell, P. J., & Lubac, B. (2010). Uncertainties of optical parameters and their propagations in an analytical ocean color inversion algorithm. *Applied Optics*, *49*(3), 369–381.

Lee, Z., Carder, K. L., & Arnone, R. A. (2002). Deriving inherent optical properties from water color: A multiband quasi-analytical algorithm for optically deep waters. *Applied Optics*, *41*(27), 23–30.

Lee, Z., Du, K., Arnone, R., Liew, S., & Penta, B. (2005). Penetration of solar radiation in the upper ocean: A numerical model for oceanic and coastal waters. *Journal of Geophysical Research*, *110*, C09019. https://doi.org/10.1029/2004JC002780

Lee, Z., Hu, C., Shang, S., Du, K., Lewis, M., Arnone, R., & Brewin, R. (2013a). Penetration of UV-visible solar radiation in the global oceans: Insights from ocean color remote sensing. *Journal of Geophysical Research: Oceans*, *118*, 4241–4255. https://doi.org/10.1002/jgrc.20308

Lee, Z., Pahlevan, N., Ahn, Y.-H., Greb, S., & O'donnell, D. (2013b). Robust approach to directly measuring water-leaving radiance in the field. *Applied Optics*, *52*(8), 1693–1701. https://doi.org/10.1364/AO.52.001693

Lee, Z. P., & Hu, C. (2006). Global distribution of Case-1 waters: An analysis from SeaWiFS measurements. *Remote Sensing of Environment*, *101*(2), 270–276. https://doi.org/10.1016/j.rse.2005.11.008

Liang, X., & Wu, L. (2013). Effects of solar penetration on the annual cycle of sea surface temperature in the North Pacific. *Journal of Geophysical Research: Oceans*, *118*, 2793–2801. https://doi.org/10.1002/jgrc.20208

Manizza, M., Le Quéré, C., Watson, A. J., & Buitenhuis, E. T. (2005). Bio-optical feedbacks among phytoplankton, upper ocean physics and sea-ice in a global model. *Geophysical Research Letters*, *32*, L05603. https://doi.org/10.1029/2004GL020778

Mobley, C. D., & Sundman, L. K. (2008). *HydroLight technical documentation*. Bellevue, WA: Sequoia Scientific, Inc. Retrieved from http://www.hydrolight.info

Morel, A. (1988). Optical modeling of the upper ocean in relation to its biogenous matter content (Case I waters). *Journal of Geophysical Research*, *93*(C9), 10749–10768. https://doi.org/10.1029/JC093iC09p10749

Morel, A., & Antoine, D. (1994). Heating rate within the upper ocean in relation to its bio-optical state. *Journal of Physical Oceanography*, *24*, 1652–1665. https://doi.org/10.1175/1520-0485(1994)024<1652:HRWTUO>2.0.CO;2

Murtugudde, R., Beauchamp, J., Mcclain, C. R., Lewis, M., & Busalacchi, A. J. (2002). Effects of penetrative radiation on the upper tropical ocean circulation. *Journal of Climate*, *15*, 470–486. https://doi.org/10.1175/1520-0442(2002)015<0470:EOPROT>2.0.CO;2

NASA (2003). *Ocean optics protocols for satellite ocean color sensor validation* (Rev. 4, Vol. III: Radiometric Measurements and Data Analysis Protocols NASA/NASA/TM-2003–21621/Rev-Vol III). Greenbelt, MD: NASA, Goddard Space Flight Space Center.

Ohlmann, J. C., & Siegel, D. A. (2000). Ocean radiant heating. Part II: Parameterizing solar radiation transmission through the upper ocean. *Journal of Physical Oceanography*, *30*, 1849–1865.

Schneider, N., Barnett, T., Latif, M., & Stockdale, T. (1996). Warm pool physics in a coupled GCM. *Journal of Climate*, *9*(1), 219–239. https://doi.org/10.1175/1520-0442(1996)009<0219:WPPIAC>2.0.CO;2

Shulman, I., Gould, R. W., Anderson, S., & Sakalaukus, P. (2017). Impact of errors in short wave radiation and its attenuation on modeled upper ocean heat content. *Journal of Applied Remote Sensing*, *11*(3), 32402. https://doi.org/10.1117/1.JRS.11.032402

Smith, R. C., & Baker, K. S. (1984). The analysis of ocean optical data. In M. Blizard (Ed.), *Ocean optics VII* (Vol. 478, pp. 119–126). Bellingham, WA: Society for Photochemical instrumentation Engineering.

Smith, R., & Baker, K. S. (1986). The analysis of ocean optical data. In P. N. Slater (Ed.), *Ocean Optics VIII* (pp. 95–107). Bellingham, WA: Society for Photochemical instrumentation Engineering.

Sweeney, C., Gnanadesikan, A., Griffies, S. M., Harrison, M. J., Rosati, A. J., & Samuels, B. L. (2005). Impacts of shortwave penetration depth on large-scale ocean circulation and heat transport. *Journal of Physical Oceanography*, *35*, 1103–1119. https://doi.org/10.1175/JPO2740.1

Wei, J., Lee, Z., Lewis, M., Pahlevan, N., Ondrusek, M., & Armstrong, R. (2015). Radiance transmittance measured at the ocean surface. *Optics Express*, *23*(9), 11826. https://doi.org/10.1364/OE.23.011826

Wei, J., Lewis, M. R., Van Dommelen, R., Zappa, C. J., & Twardowski, M. S. (2014). Wave-induced light field fluctuations in measured irradiance depth profiles: A wavelet analysis. *Journal of Geophysical Research: Oceans*, *119*, 1344–1364. https://doi.org/10.1029/2013JC009572

Werdell, P. J., Proctor, C. W., Boss, E., Leeuw, T., & Ouhssain, M. (2013). Underway sampling of marine inherent optical properties on the Tara Oceans expedition as a novel resource for ocean color satellite data product validation. *Methods in Oceanography*, *7*, 40–51. https://doi.org/10.1016/j.mio.2013.09.001

Zaneveld, J. R., Boss, E., & Barnard, A. (2001). Influence of surface waves on measured and modeled irradiance profiles. *Applied Optics*, *40*(9), 1442–1449. https://doi.org/10.1364/Ao.40.001442

Zibordi, G., D'alimonte, D., & Berthon, J. F. (2004). An evaluation of depth resolution requirements for optical profiling in coastal waters. *Journal of Atmospheric and Oceanic Technology*, *21*(7), 1059–1073. https://doi.org/10.1175/1520-0426(2004)021<1059:AEODRR>2.0.CO;2